Australian Meteorological and Oceanographic Journal 63 (2013) 65–82

The land surface model component of ACCESS: description and impact on the simulated surface climatology

E.A. Kowalczyk[1], L. Stevens[1], R.M. Law[1], M. Dix[1], Y.P. Wang[1], I.N. Harman[1], K. Haynes[1,2], J. Srbinovsky[1], B. Pak[1] and T. Ziehn[1]

[1]Centre for Australian Weather and Climate Research,
CSIRO Marine and Atmospheric Research, Australia
[2]Currently at Colorado State University, Fort Collins, CO, USA.

(Manuscript received July 2012; revised March 2013)

The land surface component of the Australian Community Climate and Earth System Simulator (ACCESS) is one difference between the two versions of ACCESS used to run simulations for the Coupled Model Intercomparison Project (CMIP5). The Met Office Surface Exchange Scheme (MOSES) and the Community Atmosphere Biosphere Land Exchange (CABLE) model are described and compared. The impact on the simulated present day land surface climatology is assessed, in both atmosphere only and coupled model cases. Analysis is focused on seasonal mean precipitation and screen-level temperature, both globally and for Australia. Many of the biases from observations are common across both ACCESS versions and both atmosphere only and coupled cases. Where the simulations from the two versions differ, the choice of land surface model is often only a small contributor with changes to the cloud simulation also important. Differences that can be traced to the land surface model include warm biases with CABLE due to underestimation of surface albedo, better timing of northern hemisphere snowmelt and smaller seasonal and diurnal temperature ranges with CABLE than MOSES.

Introduction

Land surface models have been developed for numerical weather prediction and climate modelling to provide information on surface exchange processes. They include representations of the turbulent transport of momentum, heat and water between the land surface, canopy and the atmospheric boundary layer, as well as descriptions of thermal and hydrological processes in the soil and snow. Land surface models have evolved over the last decade to improve the representation of canopy processes, especially plant physiology and the uptake of carbon. With the incorporation of biogeochemical components and, often, vegetation dynamics, some land surface models now include a fully interactive terrestrial carbon cycle (Pitman 2003).

Many land surface models also operate as 'stand-alone' models, calculating surface fluxes from prescribed meteorological forcing, with applications at single sites as well as over regions or globally. There have been a number of comparisons of land surface models in stand-alone mode (e.g. Abramowitz et al. 2008) and benchmarking systems for land surface models are being developed (Abramowitz 2012, Kumar et al. 2012, Luo et al. 2012). Comparisons of different land surface models within a single atmospheric model are less common, due to the coupling work involved. However this is being addressed by projects such as the Land Information System (LIS), which provides a software framework for land surface modelling and data assimilation (http://lis.gsfc.nasa.gov/).

This paper describes the land surface components of ACCESS contributions to CMIP5. Two different land surface models are used. We highlight the main differences between the models and discuss how the land surface influences the simulated present day model climatology. We consider both atmosphere only and coupled model simulations.

Corresponding author address: Eva Kowalczyk, CSIRO Marine and Atmospheric Research, Private Bag 1, Aspendale, Vic. 3195. Email: eva.kowalczyk@csiro.au

The ACCESS model

Two versions of ACCESS have been used to contribute simulations to CMIP5 (Bi et al. 2013). In both cases the atmospheric component of ACCESS is the UK Met Office Unified Model (UM). For ACCESS1.0 the model configuration uses HadGEM2(r1.1) atmospheric physics (Davies et al. 2005, Martin et al. 2011) and the Met Office Surface Exchange Scheme (MOSES). ACCESS1.3 uses new atmospheric physics similar to that described in Hewitt et al. (2011) and the MOSES land surface scheme is replaced by the Community Atmosphere Biosphere Land Exchange (CABLE) model. One significant difference in the atmospheric physics configurations is the choice of the PC2 cloud scheme (Wilson et al. 2008).

Both ACCESS versions include the river routing model TRIP (Total Runoff Integrating Pathways; Oki 1997) as implemented in the UM. TRIP transports runoff from land grids to the ocean or inland basins along prescribed river paths. This fresh water flux is required for the calculation of salinity and of the thermohaline circulation.

Both ACCESS versions use the GFDL[1] Modular Ocean Model (Griffies et al. 2007) configured for ACCESS (Marsland et al. 2013), the LANL[2] sea-ice model, CICE (Hunke and Lipscomb 2010) , and the CERFACS[3] OASIS coupler (Valcke 2006) .

Land surface model descriptions

Both land surface models used in ACCESS CMIP5 simulations include formulations of the physical and biophysical processes that control the exchange of momentum, radiation, heat, and water fluxes between the land surface and the surface atmosphere. However the treatment of some aspects of the exchange, especially with regard to the representation of vegetation processes, is different in each model. Both models represent surface heterogeneity using tiles to represent multiple surface types in each grid-cell. A separate energy balance is calculated for each tile to provide area-weighted grid mean fluxes and temperatures. Carbon fluxes have not been included in the ACCESS CMIP5 submissions and are not discussed here.

MOSES

A basic configuration of version 2.2 of MOSES was used in the ACCESS1.0 simulation (Cox et al. 1999, Essery et al. 2001) and is also used for ACCESS numerical weather prediction (Puri et al. 2012). The MOSES code formed the scientific core of the Joint UK Land Environment Simulator (JULES) (Best et al. 2011) which has both stand-alone and Unified Model implementations. JULES will continue to be developed while MOSES will not. MOSES includes mechanistic formulations of the physical, biophysical and biogeochemical processes that control the exchange of momentum, radiation, heat, water and carbon fluxes between the land surface and the atmosphere. The canopy is represented in the surface energy balance equation through the coupling to the soil underneath. Tiled surface temperature for both non-vegetated and vegetated tiles is viewed in MOSES as a skin temperature and is calculated from the standard surface energy balance equation. The soil underneath is not tiled and hence a homogenous soil moisture and temperature is common to all tiles within a grid cell.

CABLE

The CABLE model has been coupled to the Met Office Unified Model and is used in ACCESS1.3 simulations. CABLE is a one layer two-leaf canopy model, as described in Wang and Leuning (1998), and was formulated on the basis of the multi-layer model of Leuning et al. (1995). It accounts for turbulent exchange within the canopy (Raupach et al. 1997) and has been previously coupled to the CSIRO Conformal-cubic Atmospheric Model (CCAM) (Law et al. 2006).

The version of CABLE used in ACCESS1.3 is derived from CABLEv1.4b, originally released in 2006 and documented by Kowalczyk et al. (2006) and Wang et al. (2011). To meet the needs of ACCESS, a number of modifications have been made to CABLE v1.4b. These include (a) tiling of surface types and soil layers, (b) a revised set of vegetation types (see description below), (c) a new soil dataset based on IGBP replaced Zobler derived data set (see description below), (d) code revisions for the calculation of canopy temperature, (e) a new method for calculating screen-level variables, (f) a new partitioning of runoff, (g) conversion of excess snow on ice sheets to runoff, (h) a simplified snow albedo calculation to suit the three-hourly radiation timestep in ACCESS, (i) more consistent formulations of heat and water fluxes to ensure an acceptable surface energy and water balance in long climate simulations. We designate this version as CABLE v1.8. These modifications are also included in CABLE v2.0, which was released in late 2012.

Similarities and differences between CABLE and MOSES

The main difference between the physics of CABLE and MOSES is the representation of the canopy. In MOSES a 'horizontally tiled' approach is used in which the canopy is modelled by conceptually placing it beside bare ground. By contrast, in CABLE the canopy is conceptually above the ground allowing for the aerodynamic and radiative interaction between the canopy and the ground. The novel features in the canopy representation in CABLE which are not present in MOSES are:

- The model differentiates between sunlit and shaded leaves for the calculation of photosynthesis, stomatal conductance and leaf temperature (Wang and Leuning 1998).
- The plant turbulence model is used to calculate the air temperature and humidity within the canopy.

[1]Geophysical Fluid Dynamics Laboratory, Princeton, NJ.
[2]Los Alamos National Laboratory, Los Alamos, NM.
[3]Centre Européan de Recherche et de Formation Avancée en Calcul Scientifique, Toulouse.

Table 1. The list of structural differences in representation of canopy and soil/snow in MOSES in ACCESS1.0 and CABLE in ACCESS1.3.

	MOSES in ACCESS1.0	*CABLE in ACCESS1.3*
Canopy formulation	• One big leaf model • Canopy placed beside bare ground	• Two leaf model (sunlit and shaded leaves) • Canopy placed above the ground
Grid Tiles	9 surface types (5 vegetated) with 9 tiles used in each grid cell	13 surface types (10 vegetated) with up to 5 tiles used in each grid-cell
Soil	4 layers, no subsurface tiling	6 layers, subsurface tiling
Snow	1 layer	3 layers

- The canopy albedo is resolved diurnally as a function of beam fraction, the sun angle, canopy leaf area index, leaf angle distribution and the transmittance and reflectance of the leaves.

Both models use multiple surface types in each grid-cell (surface tiling), but with different numbers of vegetated and non-vegetated types (Table 1). Soil tiling is used in CABLE but not in MOSES. Soil processes are modelled similarly in both models but with different vertical resolution. Soil temperature and moisture are calculated for four soil layers of depths 0.1, 0.25, 0.65 and 2.0 m in MOSES and six layers of depths 0.022, 0.058, 0.154, 0.409, 1.085 and 2.872 m in CABLE. In both models soil moisture is calculated using Richards' equation with the hydraulic relationship taken from Clapp-Hornberger (1978). The evolution of soil moisture depends on the rates of infiltration, plant transpiration, soil evaporation and deep drainage. The heat diffusion equation, including an explicit freeze–thaw scheme, is solved to calculate the soil temperature profile. In CABLE soil water is assumed to be at the ground temperature so there is no heat exchange between the soil moisture and the soil due to vertical movement of water. MOSES does account for this heat exchange.

In both models snow evolution is based on the mass budget between the snowfall, sublimation and the snowmelt. Calculation of physically based snow albedo is also included. CABLE accounts for snow metamorphism through changes in snow density and explicit calculations of snow temperature and density for each of the three snow layers. The snow excess over the ice sheets was converted into runoff to prevent unrealistic snow accumulation and to approximate water discharge to the ocean from iceberg melting.

The main differences between MOSES and CABLE are summarised in Table 1.

Land surface model parameters and surface datasets

The performance of MOSES and CABLE also depends on the values of their respective parameters, many of which vary by vegetation and soil type. Both models use a number of surface datasets to derive the distributions of vegetation and soil types as well as some of the characteristics of the vegetation and soil.

Fig. 1. Soil albedo data used in ACCESS.

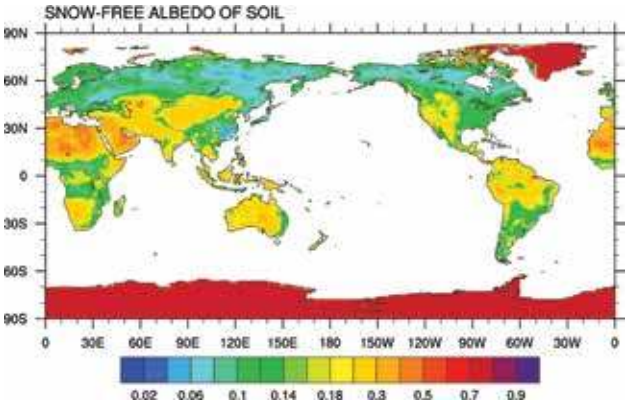

Soil datasets

Both ACCESS1.0 (MOSES) and 1.3 (CABLE) use the IGBP (Global Soil Data Task Group 2000) soil data. The hydraulic properties are determined from information on soil texture based on the empirical relationships suggested by Cosby et al. (1984), as described in Jones (2008). Each soil type is described by the following hydraulic characteristics: saturation content, wilting content, field capacity, hydraulic conductivity and matrix potential. These properties define soil water holding capacity and control the rate of water infiltration through the soil. Assumed forms of the relationship between the hydraulic properties and soil moisture content is taken from Clapp and Hornberger (1978). Soil thermal conductivity and heat capacity depend on soil moisture and ice content and affect the heat diffusion in the soil. In CABLE soil moisture is assumed to be at the ground temperature so there is no heat exchange between the soil moisture and the soil due to vertical movement of water, while in MOSES this process is represented. At the beginning of the simulation soil moisture and temperature of the tiles within a grid box are initialised to the grid values.

Both CABLE and MOSES use the same spatially varying soil albedo as shown in Fig. 1. This data set was derived by blending soil albedo from Wilson and Henderson-Sellers (1985) with MODIS derived albedo as described in Houldcroft et al. (2009); for details see Jones (2008).

Comparison of this data set with MODIS satellite measurements (Moody et al. 2005) shows that areas of the northern hemisphere high latitudes and China have snow free ground albedo of 0.04–0.08 when observed values are at least 0.1.

Vegetation distribution

ACCESS1.0 with MOSES uses five vegetated surface types (broadleaf trees, needleleaf trees, C3 grass, C4 grass and shrubs) and four non-vegetated types (urban, inland water, bare soil and ice). The spatial distribution of different surface types is derived from 0.5° by 0.5° International Geosphere Biosphere Program (IGBP) data (Loveland et al. 2000) with each of the IGBP types being interpreted as a mix of the nine MOSES surface types, with the proportions dependent on the IGBP type. The vegetation distribution used in this study is for present day conditions and does not change in time.

The implementation of CABLE in ACCESS1.3 uses ten vegetated surface types and three non-vegetated types (Table 2). The CMIP5 experiment provided a land-use change dataset (Hurtt et al. 2011) with annual values of primary vegetation, secondary vegetation, crop and pasture at 0.5° × 0.5° resolution. Determining how to map primary and secondary vegetation to the types used in CABLE is a challenging task. To assist in this process, we have used an intermediate dataset prepared for the Common Land Model 4 (CLM4; Lawrence et al. 2012). Lawrence et al. (2012) used a combination of satellite (MODIS) derived present day vegetation and a CLM4 derived potential vegetation distribution to determine the mapping of primary and secondary vegetation to CLM4 plant functional types (PFTs) over time. This dataset of CLM4 PFTs at 0.5° × 0.5° resolution was mapped to CABLE vegetated types. In general, CABLE types are the sum of one to three CLM4 PFTs, since CABLE does not differentiate types by climatic region (boreal, temperate, tropical) while CLM4 does.

From this 0.5° distribution of CABLE types, vegetation distributions were prepared for the ACCESS1.3 resolution of 1.875° × 1.25°. Since wetland and lake types were not in the CLM4 dataset available to us, these were taken from IGBP (Loveland et al. 2000), and did not change over time. Likewise permanent ice could not be determined from the available CLM4 dataset, and was taken from the ACCESS1.0 (MOSES) ice distribution.

CABLE can use any number of the available surface types within each land grid-cell; selecting the number of tiles to simulate is a compromise between providing sufficient tiles to represent mixed vegetation (e.g. savanna) and computational cost. For ACCESS1.3, the vegetation distribution was kept fixed. For all coupled model simulations, an 1850 surface-type distribution was used while for the AMIP simulation, a 2005 surface-type distribution was used. ACCESS1.3 has 10865 grid-cells with a non-zero land fraction. For each grid-cell, in addition to the fixed lake and wetland fractions, we added up to three further surface types while not allowing any land fraction smaller than five per cent of the grid-cell area. In total we simulate 21051 (21315) tiles for 1850 (2005) respectively, with 5109 (5068) grid-cells being represented by a single tile (including all grid-cells with permanent ice), 1843 (1679) by two tiles, 3451 (3641) by three tiles and 460 (477) by four or five tiles.

Figure 2 shows the vegetation distribution used in ACCESS1.0 and ACCESS1.3 (coupled runs), grouped into four broad surface type categories; trees, grass/shrubs/crops, inland water, bare ground/ice. In general the distributions are broadly similar between the two cases. The main difference between the two cases reflects the structural difference between MOSES and CABLE. CABLE accounts for bare ground underneath a canopy, and hence there are many grid-cells in the CABLE distribution without any bare ground (Fig. 2(h)). By contrast, MOSES does not account for bare ground under a canopy and every grid-cell is consequently allocated some proportion of bare ground (Fig. 2(g)). This difference is reflected in the other surface type fields, with larger maximum percentages in the tree and grass fields for CABLE than MOSES, because bare ground does not always need to be included. It is also worth noting the higher fraction of wetlands and lakes in the MOSES distribution (Fig. 2(e)) compared to the CABLE distribution (Fig. 2(f)).

Figure 3 shows crop distributions from the ACCESS1.3 coupled run (1850 distribution) and the ACCESS1.3 AMIP run (2005 distribution). The 2005 distribution shows significant expansions of cropland area. In some regions the crops mostly replace grass (e.g. Australia, North America) and in these cases the different land-use is unlikely to be significant since the characteristics of grass and crops within CABLE are similar. In Eurasia and Asia, the crops mostly replace trees. In these regions the change in surface type may have a small impact on the simulated climate.

Table 2. Surface types used in CABLE, and key parameter values. The unit is m for canopy height and leaf length, mol m^{-2} s^{-1} for the maximal carboxylation rate of the leaf (Vcmax), and dimensionless for leaf angle parameter (χ) (Wang et al. 2011).

Type	*Height*	χ	*Length*	*Vcmax*
Evergreen needleleaf	17.0	0.01	0.055	4.0e-5
Evergreen broadleaf	35.0	0.10	0.10	5.5e-5
Deciduous needleleaf	15.5	0.01	0.04	4.0e-5
Deciduous broadleaf	20.0	0.25	0.15	6.0e-5
Shrub	0.60	0.01	0.10	4.0e-5
C3 grass	0.567	–0.30	0.30	6.0e-5
C4 grass	0.567	–0.30	0.30	1.0e-5
Tundra	0.567	–0.30	0.30	4.0e-5
Crop	0.55	–0.30	0.30	8.0e-5
Wetland	0.55	0.0	0.30	5.0e-5
Bare ground	0.0	0.0	0.03	1.7e-5
Lakes	0.0	0.0	0.03	1.7e-5
Ice	0.0	0.0	0.03	1.7e-5

Fig. 2. Percentage grid-cell coverage of surface types grouped into four broad categories: trees (a,b), grass/shrubs/crops (c,d), water (e,f), bare ground/ice (g,h). ACCESS1.0 distributions (left column) are trees (a) being the sum of broadleaf and needleleaf tree types, (c) being the sum of C3 grass, C4 grass and shrub types, (e) being the water type and (g) being the sum of bare ground and permanent ice types. The small ACCESS1.0 urban fraction is not plotted. ACCESS1.3 coupled model distributions (right column) are the sum of four tree types (b), the sum of shrub, C3 grass, C4 grass, tundra and crop types (d), the sum of wetland and lakes types (f) and the sum of bare ground and permanent ice types (h).

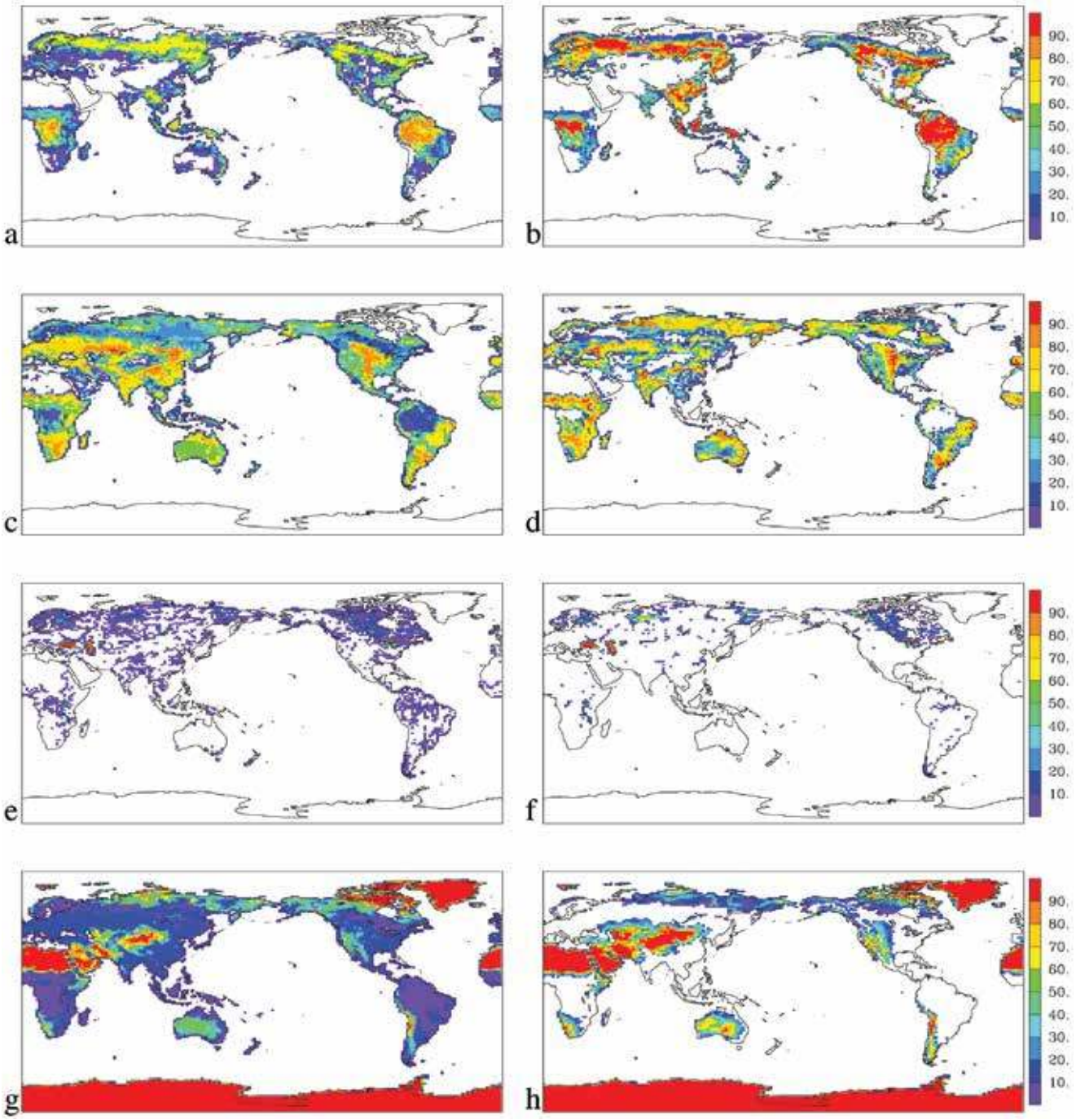

Vegetation parameters

The key parameters for each CABLE surface type used in the ACCESS1.3 simulations are given in Table 2. Canopy height is used for roughness length calculations while leaf angle and length are used for calculating radiation absorption and leaf boundary conductance, respectively. Vcmax controls the maximal carbon assimilation and stomatal conductance (see Wang et al. 2011). Wetlands and lakes are modelled very simply in this version of CABLE; both are treated as permanently saturated land surfaces with wetlands using grass-like parameters while lakes use bare-ground parameters. This additional water is not balanced locally

Fig. 3. Percentage grid-cell coverage of the crop surface type for (a) the ACCESS1.3 coupled runs and (b) the ACCESS1.3 AMIP run.

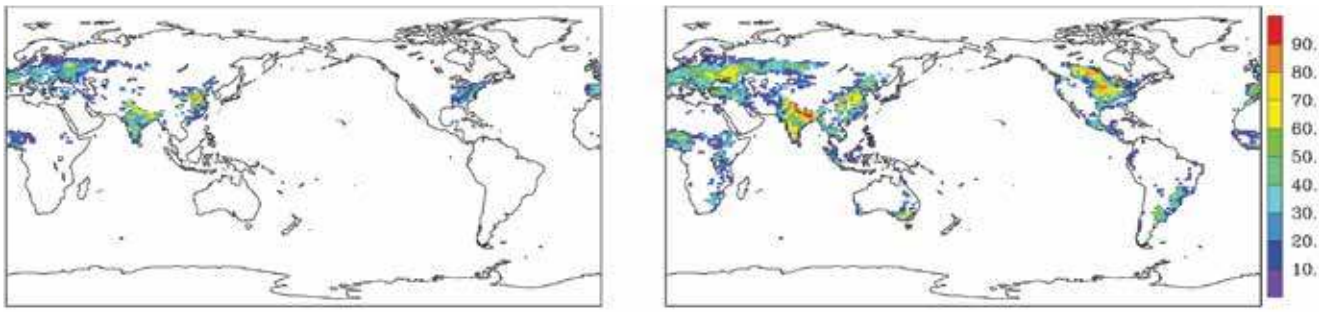

but a global adjustment is made to runoff. Parameters for the reflectance and transmittance of leaves also vary with different vegetation types. These and soil albedos were calibrated using the estimates of snow-free surface albedo from a MODIS product (Moody et al. 2005). The estimated soil albedos were subsequently found to be incompatible with the soil albedo field used in ACCESS1.3 (see Fig. 1) which has resulted in underestimated total albedo from CABLE in some regions. Another factor contributing to CABLE's low surface albedo is too low a value of reflectance coefficient for the diffuse infrared radiation. The calculated surface albedo field will be shown in the AMIP results section.

Description of vegetation parameters used by MOSES can be found in Cox et al. (1999), Cox (2001) and Jones (2008).

Leaf area index and canopy height

Both MOSES and CABLE are able to calculate canopy leaf area index (LAI) when coupled to appropriate sub-models that simulate plant growth—TRIFFID (Cox 2001) for MOSES, CASA-CNP (Wang et al. 2010) for CABLE. However these sub-models are not used in the ACCESS simulations described here and LAI and vegetation height are prescribed. MOSES uses monthly varying LAI which varies with vegetation type and canopy height which varies spatially but not in time.

CABLE used monthly varying leaf area index (LAI) taken from MODIS satellite estimates (Yang et al. 2006). However, unlike MOSES, a constant value is used across all tiles within a grid-cell. This consequently limits the differentiation of vegetated surfaces within a grid-cell, a limitation that needs to be addressed in future implementations of CABLE in ACCESS. The prescribed LAI will also act to minimise differences due to the two different vegetation distributions used in ACCESS1.3 (pre-industrial or present day). Minimum LAI values were also specified for each vegetation type.

The ACCESS1.3 implementation of CABLE reads spatially explicit canopy heights from an input file but this was set as constant for each vegetation type by using an input file with no spatial or temporal variation of canopy heights within each vegetation type. For non-vegetated surfaces the canopy height is set to zero in CABLE.

Model simulations

The set of simulations performed with ACCESS1.0 and ACCESS1.3 is described in Dix et al. (2013). Here we focus on results from two experiments with each version of ACCESS; the atmosphere only 'AMIP' simulations which we denote 1.0A and 1.3A, and the coupled 'historical' simulations which we denote 1.0C and 1.3C. Our analysis considers only the 1979–2005 period. In both cases, global atmospheric CO_2 is prescribed, increasing from 337 ppm in 1979 to 379 ppm in 2005. In the AMIP run, sea surface temperature and sea-ice is also prescribed.

Land surface climatology

Land surface models calculate surface fluxes of radiation, heat and moisture. However, these fields have not been routinely observed at global and decadal scales. Hence, we choose to focus our assessment of the land surface climatology on the seasonal means of screen-level temperature and precipitation for present day conditions. Annual means for present day conditions are presented in Bi et al. (2013) and Rashid et al. (2013).

We calculate means for December–February and June–August for 1979–2005 from the atmosphere only (AMIP) simulation and the historical coupled simulation. In general, we compare modelled fields with the ERA-Interim reanalysis product (Dee et al. 2011) and plot the bias between modelled and reanalysis fields. Taking ERA-Interim to represent observations introduces some uncertainty into the comparison, as would any other product used to represent the observations. However it is unlikely that the large-scale differences shown here would be substantially altered by using a different product. For Australia we also use quality controlled Bureau of Meteorology data sets of precipitation, minimum and maximum temperatures. We examine the biases globally, and focused on Australia.

In comparing ACCESS1.0 and ACCESS1.3 simulations, it is important to note that the choice of land surface model is only one of the differences between the simulations. In particular, ACCESS1.3 uses the PC2 cloud scheme (Wilson et al. 2008) with modifications by Franklin et al. (2012) and ACCESS1.0 uses a scheme as described in Smith (1990). Clouds play an important role in the earth's hydrological and energy cycles.

Fig. 4. Seasonal mean precipitation biases (mm/day) for ACCESS1.0 (a,b) and ACCESS1.3 (c,d) AMIP simulations evaluated against ERA-Interim analysis for December/January/February (left column) and June/July/August (right column). The model precipitation difference, ACCESS1.3 minus ACCESS1.0, is shown in (e,f).

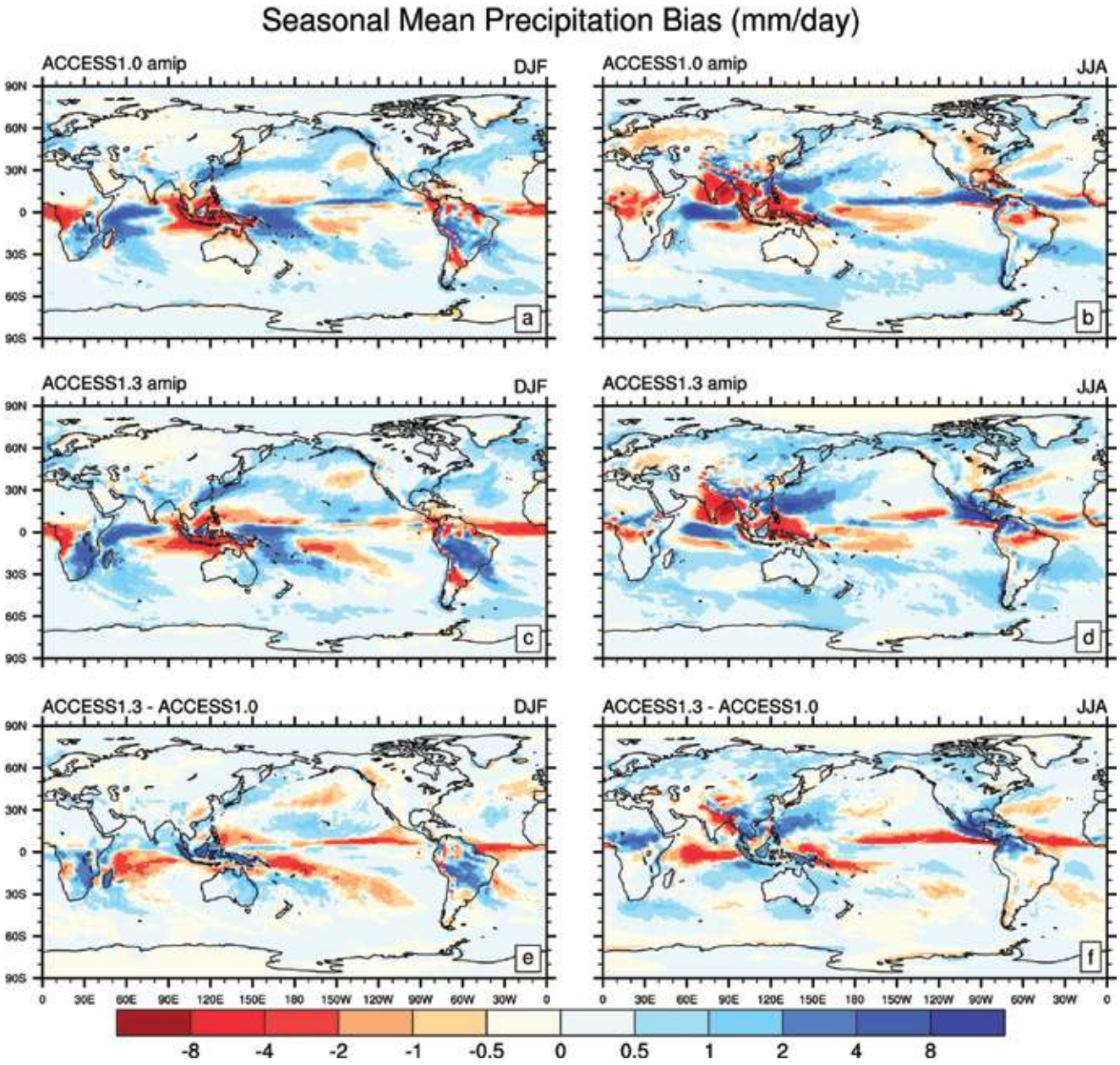

They are a precursor for the generation of precipitation which replenishes the soil moisture and so influences evaporation. Clouds reflect the incident solar radiation and absorb outgoing long-wave radiation, strongly affecting the surface energy budget and so influencing evaporation, which in turn influences cloud formation (Bierkens et al. 2008). The net effect of these complicated interactions between clouds and the earth's surface in ACCESS1.0 and 1.3 will need to be assessed in a separate study using a different experimental design. Overall, the PC2 scheme produces slightly more clouds than does the Smith (1990) scheme. Franklin et al. (2013) compared ACCESS1.3 AMIP modelled cloud properties with the CALIPSO observations concluding that the globally averaged cloud cover in the model is close to the observed. However there are important differences in the cloud distribution and mid level clouds are significantly underestimated across the tropics.

AMIP simulation

We first consider the atmosphere only simulations. Using prescribed sea surface temperature and sea-ice should constrain the climatology and aid in interpreting the differences between ACCESS1.0 and ACCESS1.3 simulations. We will also examine common biases in the simulations, which are due to similarities in the land surface

Fig. 5. Seasonal mean screen temperature biases (°C) for ACCESS1.0 (a,b) and ACCESS1.3 (c,d) AMIP simulations evaluated against ERA-Interim analysis for December/January/February (left column) and June/July/August (right column). The model screen temperature difference, ACCESS1.3 minus ACCESS1.0, is shown in (e,f).

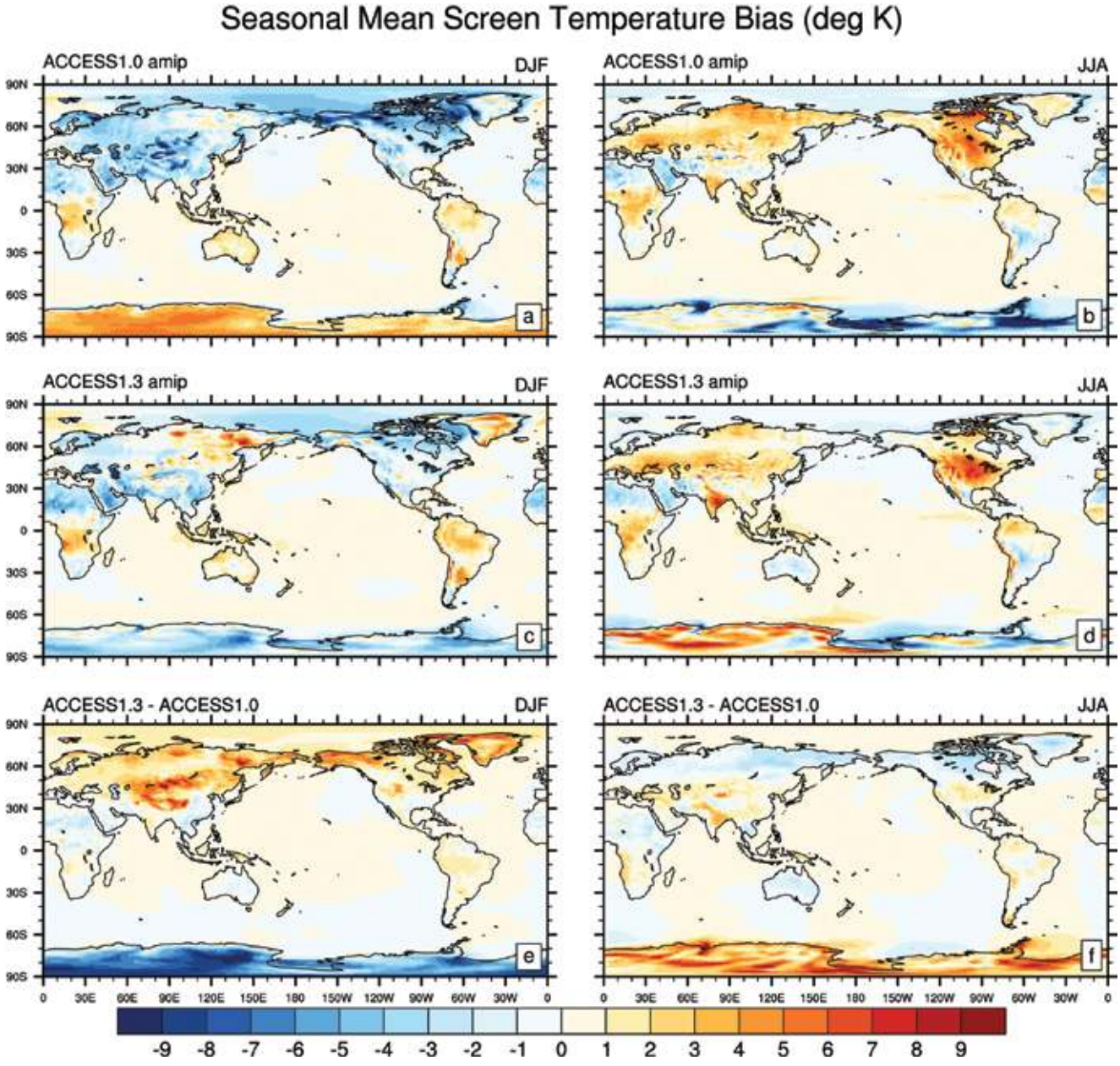

model formulations or atmospheric model weaknesses shared in both versions of the ACCESS model.

Evapotranspiration requires energy and has a strong cooling effect; it has been estimated by Shukla and Mintz (1982) that the northern hemisphere temperature would be 15–25 °C warmer under conditions of zero terrestrial evapotranspiration. Evapotranspiration from the land surface also depends on the land surface characteristics and their representation in the model as these modify the return of moisture to the atmosphere. However, the main driver of evapotranspiration is precipitation. Comparison of the seasonal precipitation biases in the AMIP simulations, 1.0A and 1.3A (Fig. 4), shows similar patterns and sign of the biases over most of the land areas. Common dry biases occur in the Amazon, equatorial Africa in DJF, an area of north Argentina in DJF and central Europe in JJA. In both simulations the Indian monsoon is severely under-predicted resulting in negative precipitation biases in JJA and an insufficient evapotranspiration. There are also common strong wet biases mainly in DJF in the southeastern part of Africa and the central part of South America, these biases are stronger in 1.3A (Fig. 4(e)) . Wet biases occur in 1.3A but not 1.0A for eastern Australia in DJF (discussed further below) and for equatorial Africa in JJA.

Fig. 6. Bar chart of seasonal mean screen temperature biases over the land for different latitude bands: Glob – all land; hNLat – high north latitude band (66°N to 90°N); mNlat – mid north latitude band (23°N to 66°N); Trop – tropics (23°S to 23°N); mSlat – mid south latitude band (23°S to 66°S); and hSLat – high south latitude band (66 °S to 90°S), for ACCESS1.0 (white) and ACCESS1.3 (grey) AMIP simulations. The seasons are DJF (a), MAM (b), JJA (c), SON (d).

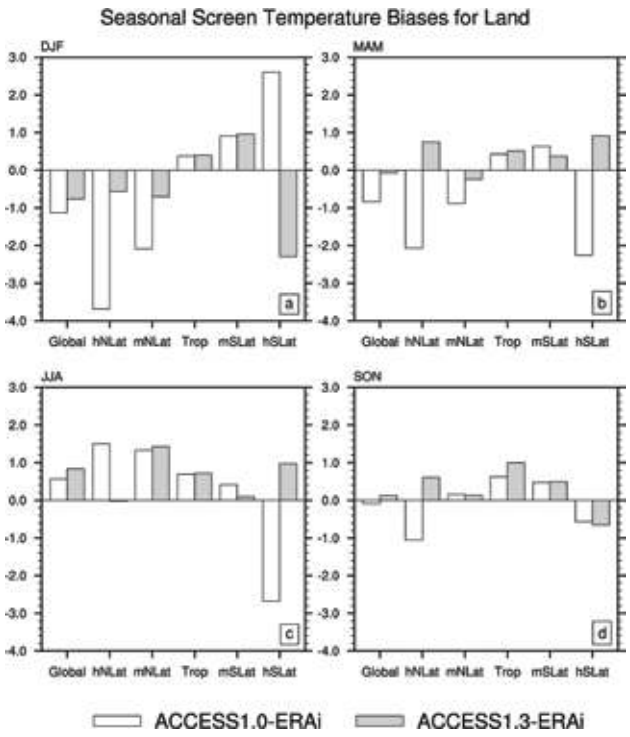

Figure 5 shows the mean screen-level temperature biases for winter and summer while biases over land area are quantified for different latitude bands in Fig. 6. As for precipitation, the pattern and sign of the bias is similar across simulations for most land areas with a few exceptions including Antarctica, northeast Asia and the Himalayas. In JJA there are common warm biases across central Eurasia, North America and the Indian peninsula, related to the underestimation of precipitation in these regions. Likewise, the underestimation in rainfall seen in both simulations in equatorial Africa in DJF induces the warm temperature biases in this region. This is enhanced further by a positive feedback between the decrease in evapotranspiration and increased solar radiation due a deficit in cloud cover. For example the warm bias in central North America in 1.3A coincides with 30 per cent underestimation of cloud cover in the area (Franklin et al. 2013).

Over a large part of the northern hemisphere in DJF, screen-level temperature simulated in 1.0A is lower than in 1.3A by up to several degrees (Fig. 6(a)). One of the contributing factors is the calculation of albedo by CABLE; for vegetated surfaces, including canopy protruding through snow, the canopy albedo acts to decrease the underlying albedo from the soil/snow, resulting in areas with vegetation cover having lower surface albedo in CABLE than MOSES (Fig. 7). More radiation is consequently absorbed so that CABLE is warmer than MOSES. The impact of the different albedo can also be seen in DJF in the southern hemisphere where 1.3A is slightly warmer in the Amazon basin, due to a significantly lower albedo (0.06 to 0.1) compared to 1.0A (0.14 to 0.18).

However differences in surface albedo cannot explain all the temperature differences since 1.0A is generally warmer in JJA over high latitude northern land (Fig. 6(c)); even though it has higher albedo than 1.3A i.e. albedo used in MOSES is in the range 0.08 to 0.16 versus 0.05 to 0.1 in CABLE (Fig. 7). It is likely that differences in the atmospheric physics settings are contributing to the warmer bias in 1.0A compared to 1.3A in JJA. It is worth noting that in 1.0A the cold bias over northern land in winter and the warm bias in summer means that the seasonality of screen-level temperature is overestimated.

The 1.3A simulation tends to have a warm bias especially in mountainous snow covered regions. For example, in east Siberia where the mean DJF temperature drops to below –20 °C, 1.3A overestimates the minimum daily temperature. 1.3A gives a similar bias in JJA over Antarctica, where the minimum temperature is overestimated over high topography. Unexpectedly, 1.0A shows a strong positive temperature bias over Antarctica in DJF (Fig. 6(a)). This appears to be due to MOSES rather than to differences in the atmosphere settings between ACCESS1.0 and ACCESS1.3 since a short (five year) AMIP simulation with ACCESS1.0 atmosphere settings and CABLE (1.1A) did not show any warming in the Antarctic in DJF.

One of the consequences of the temperature difference between 1.0A and 1.3A in boreal winter and spring in the northern hemisphere high latitudes (Fig. 6 (a), (b)) is the timing of the calculated snowmelt and runoff. Spring snowmelt is an important source of water to replenish soil water reservoirs, with an excess of water diverted to runoff. Modelled spring and summer runoff is shown in Fig. 8. In 1.3A generation of runoff from snowmelt begins in March, increasing rapidly in April, and reaches a maximum in May when the snow is melting at the fastest rate. This timing of snowmelt agrees with observations presented in Tan et al. (2011) showing that the snowmelt season starts in the southern part of the Eurasian Arctic around mid March and by mid May snow is melted. In 1.3A the snowmelt cannot penetrate frozen soil and thus flows on the surface along topography as surface runoff (Fig. 8(c)). The runoff slowly declines in the following months being sustained only by summer precipitation (Fig. 8(d)). In 1.0A in the high latitudes significant snow melting begins in April and continues through May; however a substantial amount of runoff is not generated until late May, reaching a maximum in June (Fig. 8(b)). This is because in 1.0A snowmelt water enters partially unfrozen soil and drains slowly through the soil column before emerging as runoff from the lower part of the soil column.

Fig. 7. Seasonal mean surface albedo for ACCESS1.0 (a, b) and ACCESS1.3 (c, d) AMIP simulations for December/January/February (left column) and June/July/August (right column).

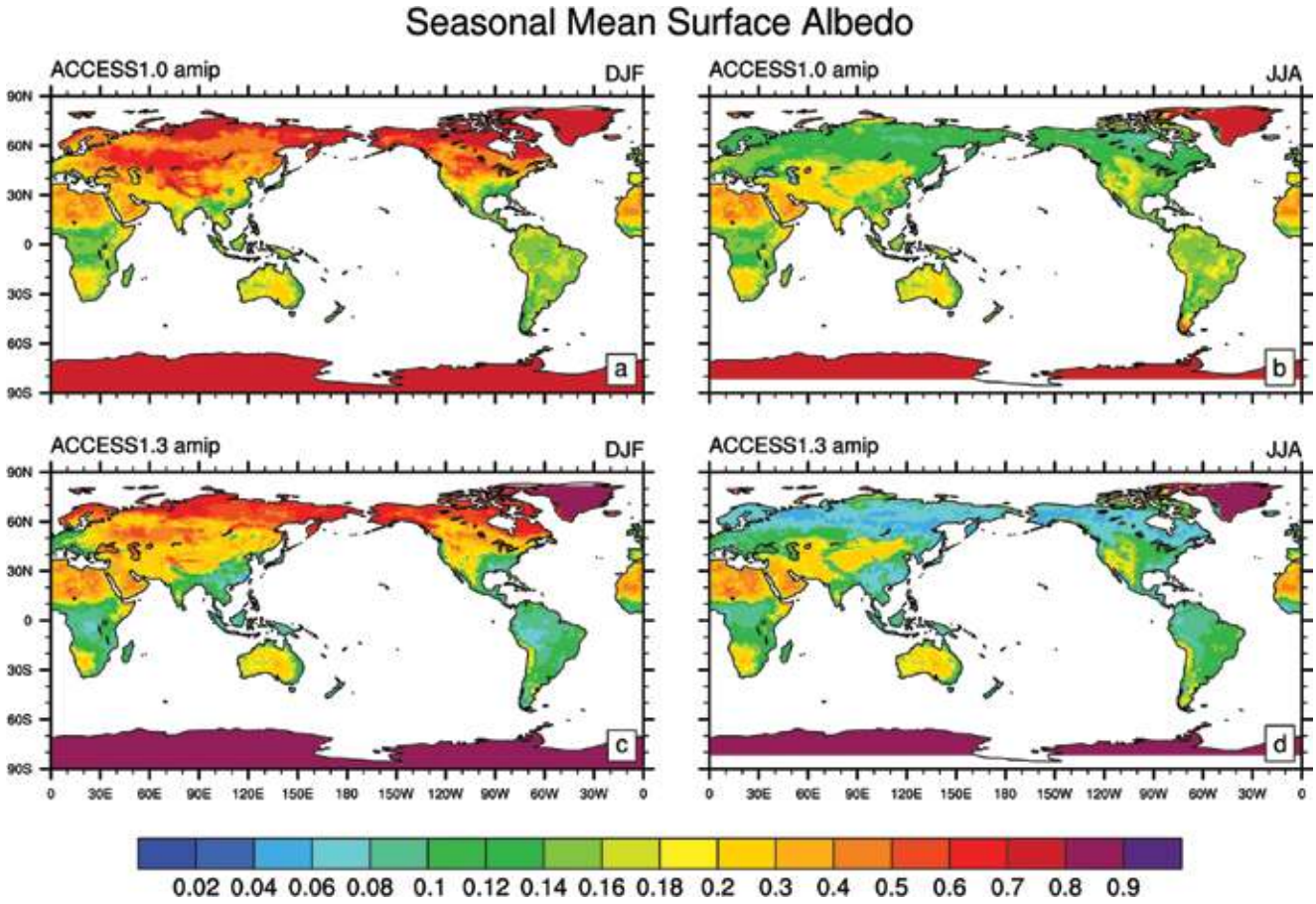

Tan et al. (2011) depicted the seasonality of the observed stream flow from the Lena, Yenisei and Ob rivers which contribute about half of the total fresh water flux to the Arctic sea. In four out of five presented hydrographs the stream flows increased rapidly in April reaching a maximum in late April or May before a decline. This suggests that the 1.3A runoff timing may be more consistent with the observations than 1.0A.

Table 3 summarises 1.0A and 1.3A annual mean temperature, precipitation, water and energy budget components with estimates from Baumgartner and Reicher (1975), Henning (1989), Legates and Wilmot (1990) and Smith et al. (2008) for land surface only. Overall 1.3A simulation produced a slightly warmer and wetter climate. Net radiation over the land is lower by 2.9 W m^{-2} in 1.3A than in 1.0A in spite of lower values of land surface albedo (Fig. 7). This is indicative of higher cloud cover over the land in 1.3A and is consistent with higher precipitation in 1.3A. Along with the slightly warmer surface temperatures in 1.3A, this leads to increased evaporation and runoff. The lower net radiation flux and higher evapotranspiration results in a lower value of the sensible heat flux over the land and larger latent heat flux.

Table 3. Water and energy budget components, averaged over all land surfaces for 1.0A and 1.3A compared to estimates from other sources.

	1.0A	*1.3A*	*Other estimates*
Precipitation (mm/day)	2.13	2.57	2.03[a], 2.05[b]
Evaporation (mm/day)	1.49	1.68	1.31[a]
Surface runoff (mm/day)	0.23	0.18	0.73[a]
Drainage (mm/day)	0.51	0.79	
Screen temperature (°C)	8.75	9.15	8.5[c]
Sensible heat (W m^{-2})	31.41	23.96	30.53[d] ,37.31[e]
Latent heat (W m^{-2})	43.37	48.81	35.86[d], 34.41[e]
Net radiation (W m^{-2})	77.68	74.79	66.39[d], 72.20[e]

[a]Baumgartner and Reichel (1975); [b]Legates and Willmott (1990); [c]Smith et al. (2008); [d]Henning (1989); [e]Budyko (1978)

Fig. 8. Seasonal mean total runoff (mm/day) for ACCESS1.0 (a, b) and ACCESS1.3 (c, d) AMIP simulations for March/April/May (left column) and June/July/August (right column).

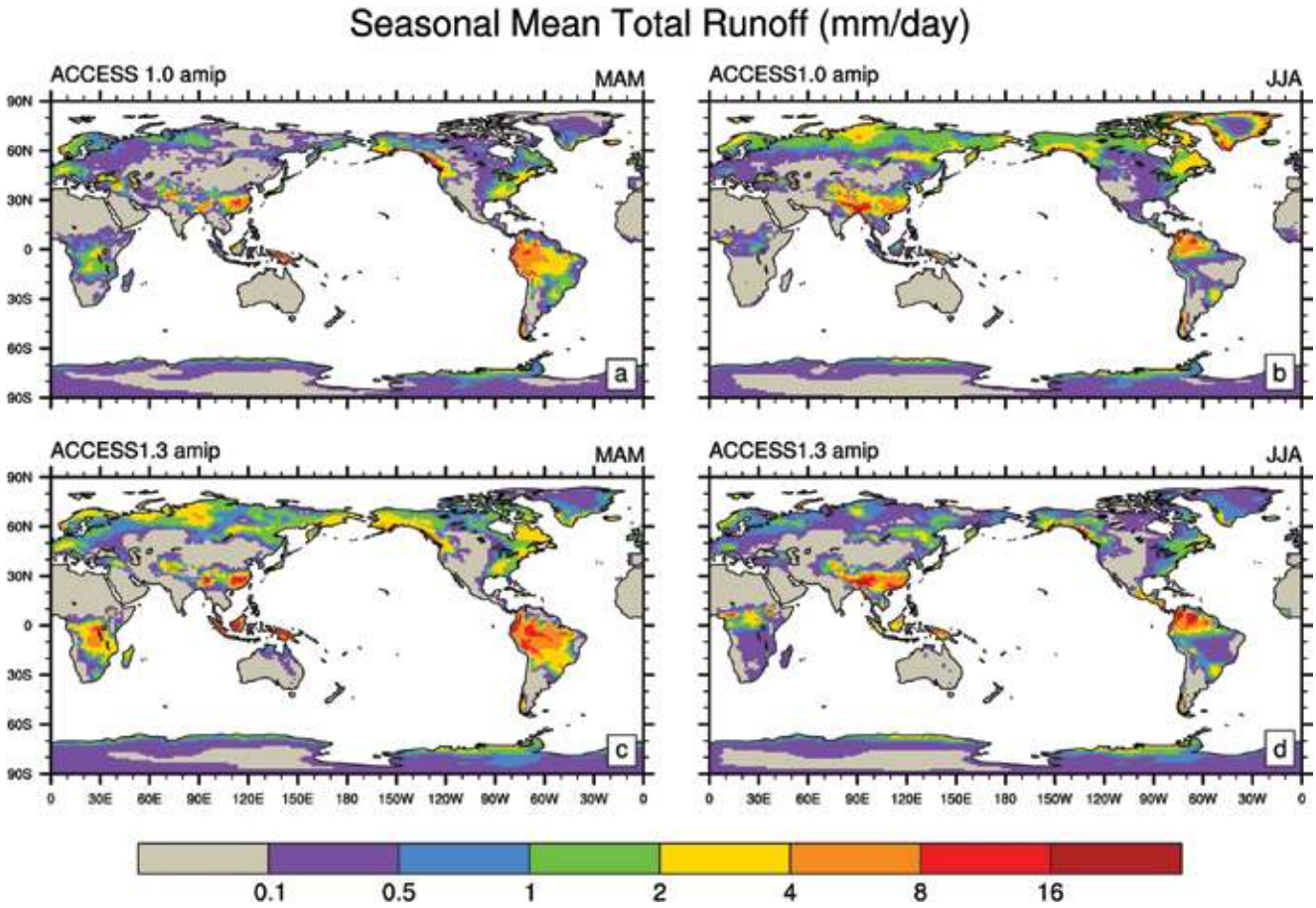

On the other hand net radiation over the ocean is higher by about 3.2 W m^{-2} in 1.3A than 1.0A indicating lower cloud cover. The differences in the cloud amount and distribution between 1.0A and 1.3A, due to the different cloud parameterisation schemes used here, warrants further investigation in simulations run with the same atmospheric settings.

Coupled model: historical simulation

The coupled model simulations of the historical period are analysed in the same manner as the AMIP simulations, focusing on the biases in precipitation and screen-level temperature for the winter and summer seasons averaged over 1979–2005. We consider how the ocean model simulation of sea surface temperature impacts on the land surface climatology by comparing the AMIP and coupled model cases.

Precipitation biases for the 1.0C and 1.3C simulations are shown in Fig. 9. Comparison with the corresponding AMIP precipitation biases (Fig. 4) shows that the pattern and sign of the biases over the land areas are mostly similar while there are significant differences in precipitation patterns and intensity over the oceans. Focusing on the land regions, the Indian monsoon is under-predicted in the coupled runs as for the AMIP cases, with negative precipitation biases over India in JJA. The bias appears to be less severe for 1.0C compared to 1.0A while there is little change between 1.3C and 1.3A. In JJA the dry bias in the central-eastern part of North America is reduced in the coupled runs compared to the AMIP simulations. There is some tendency to drier conditions in the Amazon in DJF in the coupled model case, more noticeably in 1.3C than in 1.0C. 1.3C also shows an increased dry bias north of the equator in Africa, but a reduced dry bias south of the equator relative to 1.3A. The dry bias stretching from north Australia across the maritime continent to South East Asia in the AMIP run (Fig. 4) has been partially replaced by a strong wet bias in both coupled model cases.

The screen-level temperature biases for 1.0C and 1.3C (Fig. 10) are very similar to those from the AMIP simulations over land. Notable differences include (a) an increased warm bias in DJF over Antarctica in 1.0C associated with a positive bias in simulated SST around this continent, (b) a warm bias in central North America in DJF in 1.3C associated with a positive SST bias off the east coast of North America, (c) an increased warm bias in the Amazon in DJF, more obvious in 1.3C than 1.0C, associated with decreased rainfall, (d) a reduction in the warm bias in India in JJA in 1.0C associated

Fig. 9. Seasonal mean precipitation biases (mm/day) for ACCESS1.0 (a, b) and ACCESS1.3 (c, d) historical simulations evaluated against ERA-Interim analysis for December/January/February (left column) and June/July/August (right column). The model precipitation difference, ACCESS1.3 minus ACCESS1.0 is shown in (e, f).

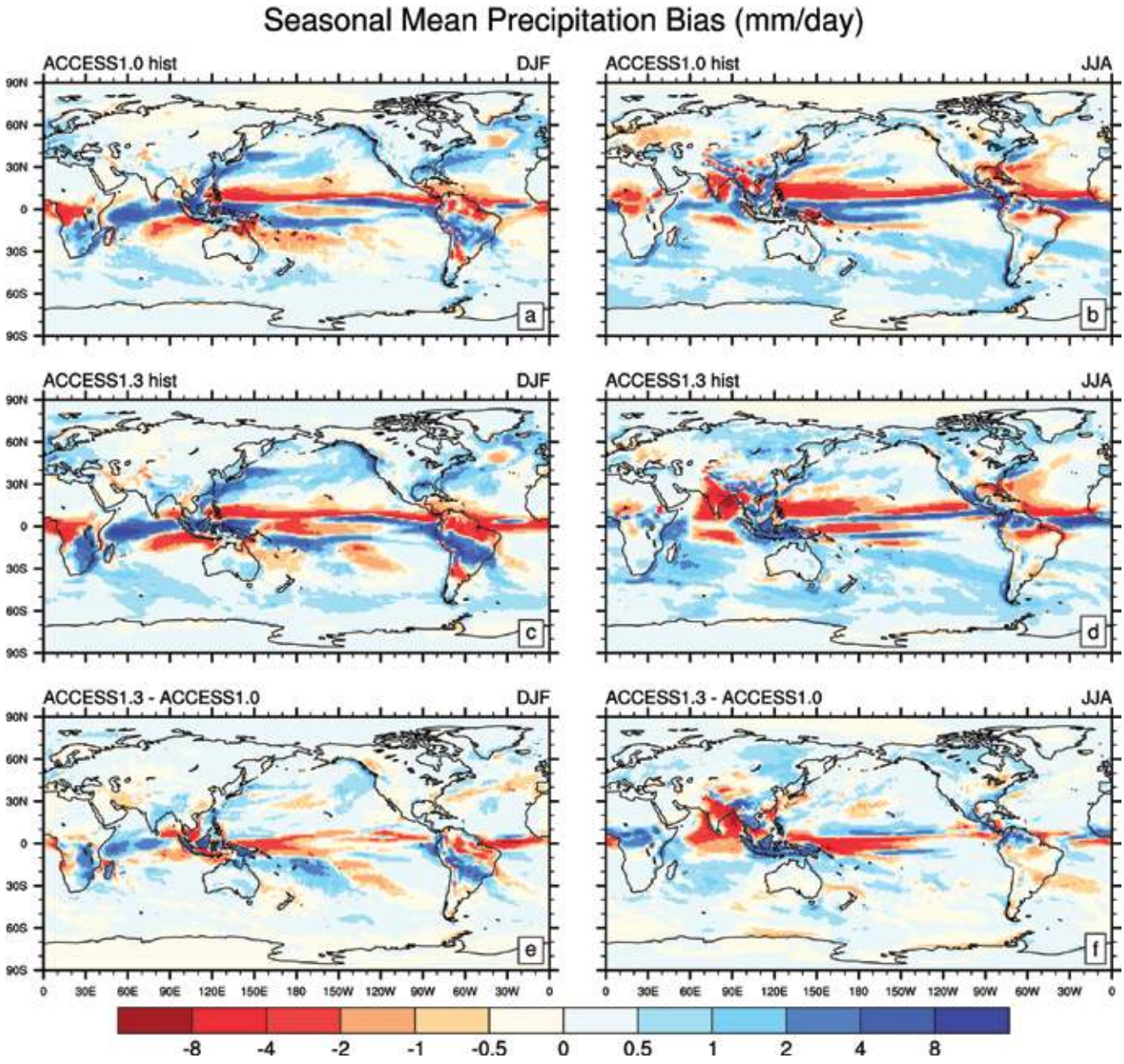

with a small improvement in rainfall there and (e) a general reduction in the warm biases in JJA over the northern hemisphere in conjunction with cooler SST temperatures in the low latitudes of the Pacific and Atlantic oceans, and increased rainfall in e.g. North America. Common warm biases remain in both 1.0C and 1.3C simulations in Eastern Europe (in JJA) and equatorial Africa, the last one a bit stronger in 1.3C than 1.0C due to lower CABLE surface albedo (0.08 to 0.12) compared to MOSES (0.12 to 0.16). As in the AMIP simulations the timing of the calculated snowmelt and runoff in 1.3C run occurs about a month earlier than in 1.0C.

Precipitation and screen temperature biases over Australia

Rainfall over Australia is strongly affected by sea surface temperature as well as other climatic and weather drivers (Risbey et al. 2011). Hence, we first compare the AMIP style simulations, 1.0A and 1.3A, to observations, thus excluding any effects of the coupled model calculated SST anomalies and associated feedbacks between the ocean and the atmosphere. In this analysis we use precipitation observations from the Australian Bureau of Meteorology (2000).

The mean modelled and observed seasonal rainfall for austral summer and winter is presented in Fig 11. Overall, the model is capturing well the seasonal patterns of rainfall.

Fig. 10. Seasonal mean screen temperature biases (°C) for ACCESS1.0 (a,b) and ACCESS1.3 (c,d). Historical simulations evaluated against ERA-Interim analysis for December/January/February (left column) and June/July/August (right column). The model screen temperature difference, ACCESS1.3 minus ACCESS1.0 is shown in (e,f).

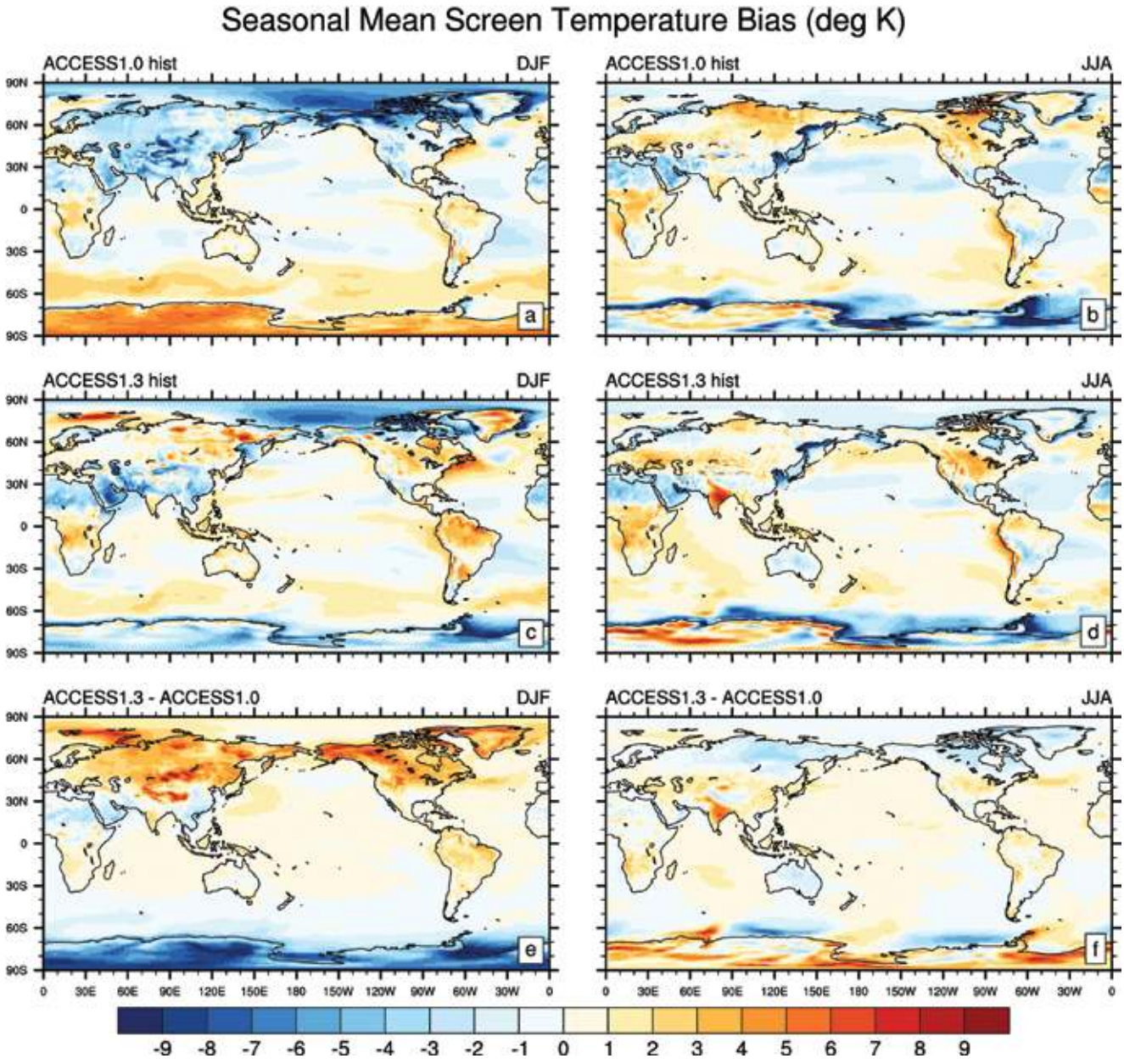

However there are some noticeable differences. In 1.0A in DJF monsoonal precipitation is less intense than observed and the rainfall along the east coast is also underestimated. Summer precipitation in the 1.3A simulation is more intense than in 1.0A and slightly larger than observed in the centre of the continent but in both simulations the extent of penetration of the monsoonal rainfall over the Great Sandy Desert in the northwest part of the continent is limited.

In winter, in both models, precipitation patterns are similar to observations but precipitation over southwestern Australia is too low and the rainfall associated with flow over topography is absent in southeastern Australia and Tasmania. The rainfall gradient across Tasmania is also largely absent in DJF, again due to the inadequate representation of topography. This problem is also seen in the simulated climate by most other climate models at this relatively coarse spatial resolution; maximum elevation in SE Australia in these ACCESS versions is only 500–600 m while in reality the Great Dividing Range has peaks over 2000 m.

Australian precipitation from the coupled model simulations is shown in Fig. 12. The patterns of precipitation are very similar to the AMIP runs but overall there is more precipitation in both 1.0C and 1.3C in both seasons in the centre of the continent but not in the coastal areas and Cape York Peninsula. In 1.3C the more intense summer rainfall along the east coast has retreated showing that the more

Fig. 11. Australian mean seasonal precipitation (mm/day) for ACCESS1.0 (left column), ACCESS1.3 (middle column) AMIP simulations and Bureau of Meteorology observations (right column) for December/January/February (a, b, c) and June/July/August (d, e, f).

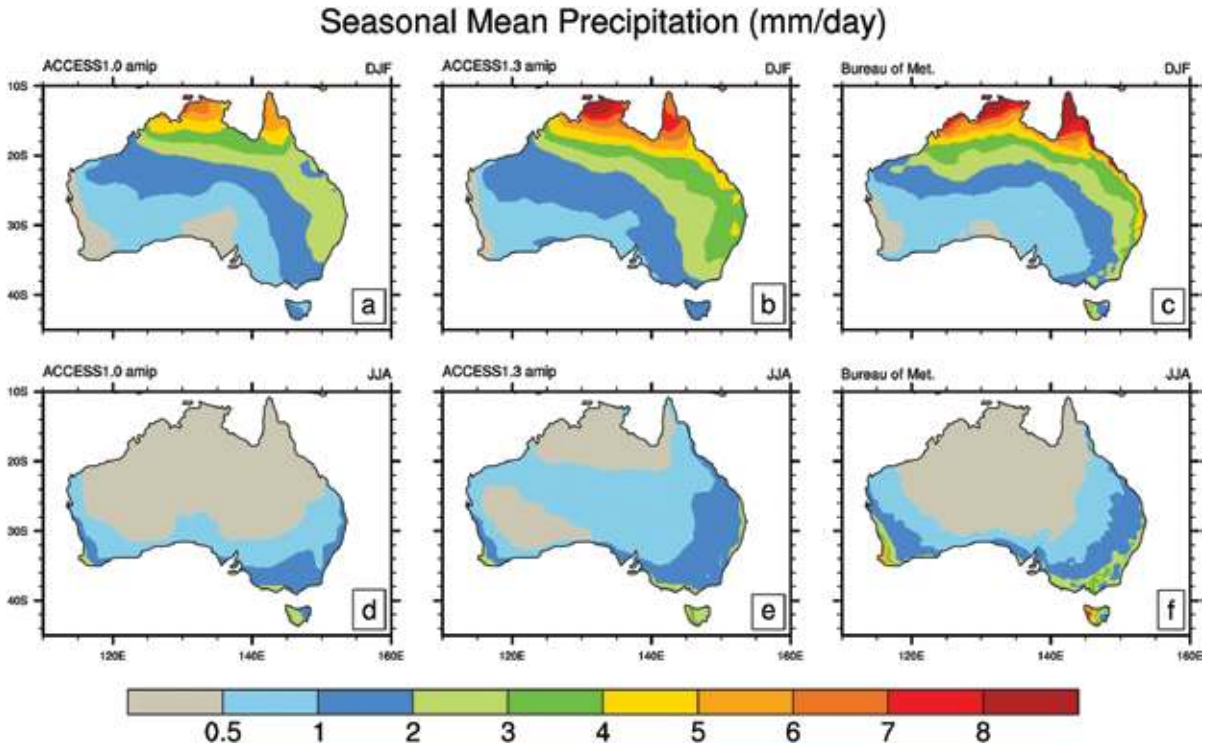

Fig. 12. Australian mean seasonal precipitation (mm/day) for ACCESS1.0 (left column), ACCESS1.3 (middle column) historical simulations and Bureau of Meteorology observations (right column) for December/January/February (a, b, c) and June/July/August (d, e, f).

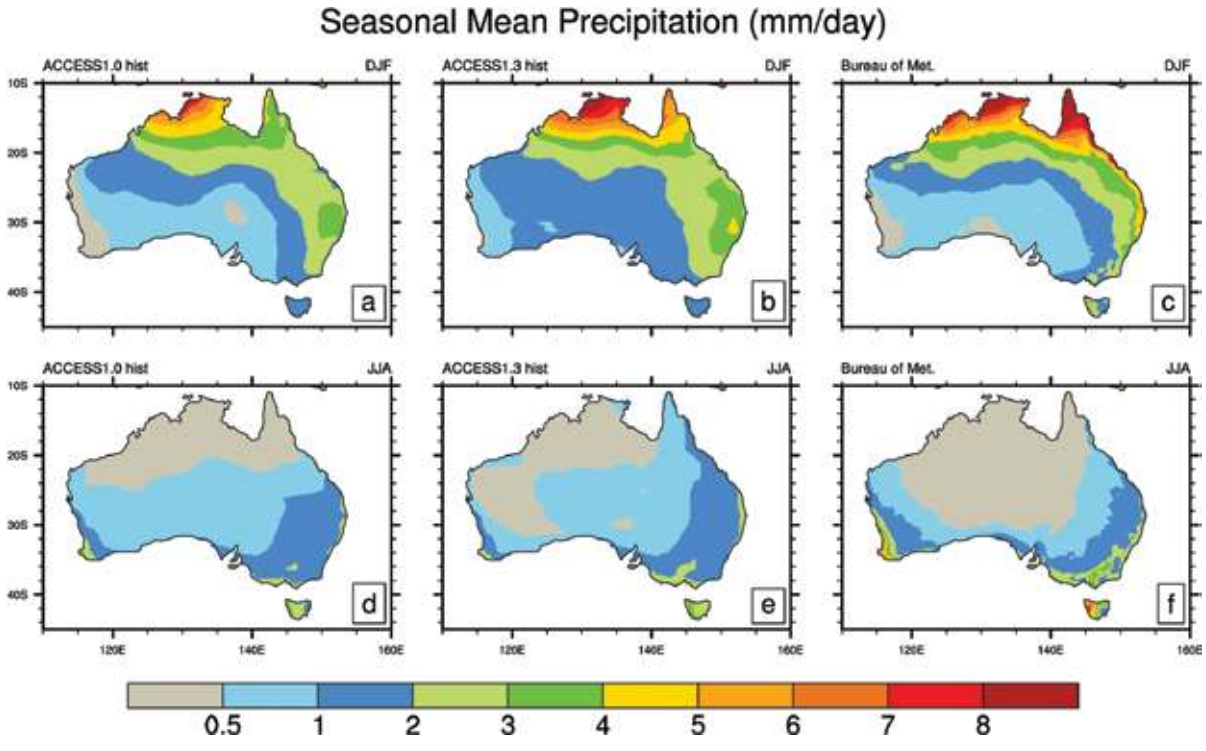

Fig. 13. Australian mean seasonal screen temperature (°C) for ACCESS1.0 (left column), ACCESS1.3 (middle column) AMIP simulations and ERA-Interim analysis (right column) for December/January/February (a, b, c) and June/July/August (d, e, f).

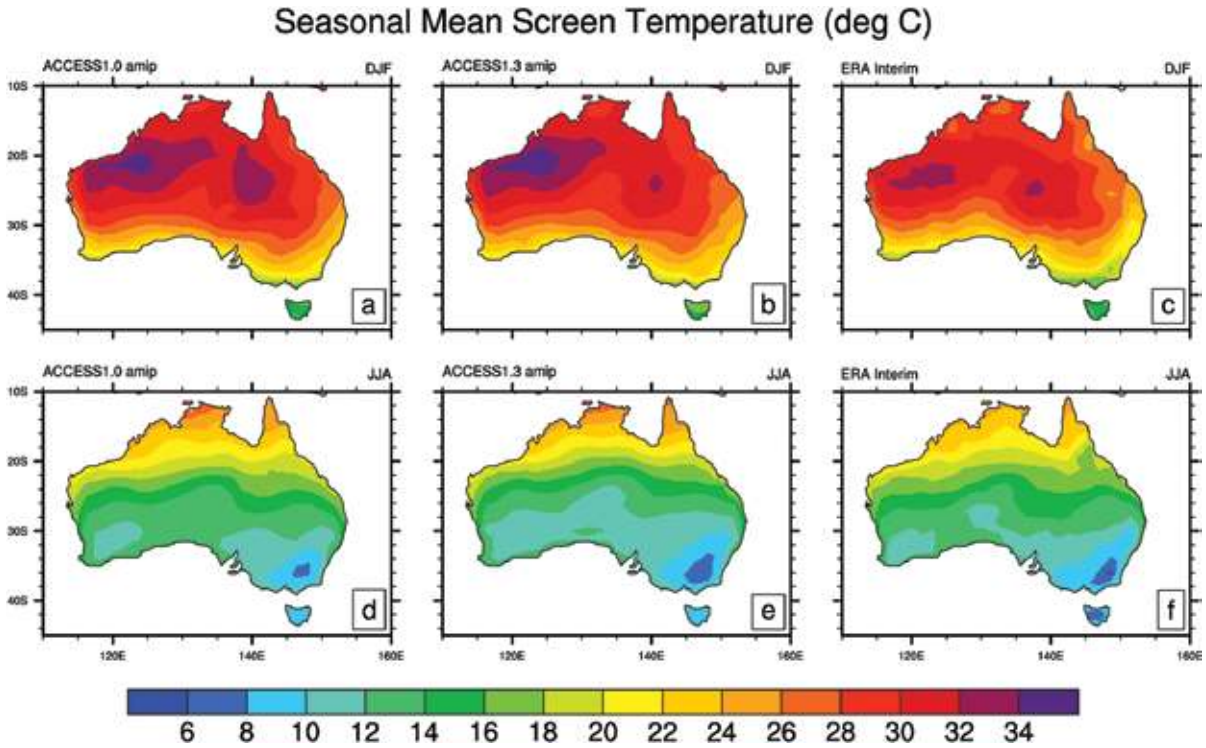

intense easterly flow events generating the rainfall (Risbey et al. 2011) are not captured by the coupled model.

Figure 13 compares the simulated mean screen-level temperature from the AMIP simulation with ERA-interim reanalysis. Overall there is a good agreement with observed temperature patterns in both seasons although both simulations are slightly too warm in the summer months. In 1.3A the simulated cloud cover over most of the continent in summer is underestimated by up to 40 per cent as compared with the CALIPSO observations (Franklin et al. 2013). The cloud underestimation by 1.3A in the north of the continent and along the east coast is consistent with the warm temperature biases in those regions and is due to not enough high and mid-level cloud, which suggests that there is not enough convection in the model in summer in these regions. In winter the clouds in 1.3A are overestimated in the centre of the continent and underestimated along the north and east coast, which is consistent with a cold temperature bias in the centre and slight warm bias along the east coast. The overestimate of cloud cover in the central region is due to too much low cloud in the model.

Figure 14 shows that the diurnal amplitude range is larger for 1.0A than 1.3A. The 1.3A results are more consistent with the diurnal amplitude from ERA-Interim while the 1.0A results are more consistent with the Bureau of Meteorology temperature dataset. It is possible that part of this difference is due to how each model derives screen-level temperature. The large differences in diurnal amplitude between 1.0A and 1.3A warrant further investigation.

For screen-level temperature, the coupled model simulations 1.0C and 1.3C are very similar to the AMIP simulations and hence are not shown.

Conclusion

This study has compared the simulated precipitation and screen-level air temperature by ACCESS1.0 and ACCESS1.3 for present day conditions in both atmosphere only and coupled model configurations. For land regions globally, the four simulations show similar biases in both magnitudes and locations as compared to the ERA-Interim reanalysis product. For example, the screen-level air temperature is overestimated in summer over most land regions, and underestimated in both winter and summer in the Sahara and Arabian Peninsula. Monsoon rainfall is underestimated particularly in India, but also in northern Australia, which may cause warm biases in these regions. Rainfall is also underestimated and screen-level air temperature is overestimated in equatorial Africa.

There are also differences among the four simulations. Some of these are consistent with differences between the two land surface components of the two ACCESS versions; others are more likely driven by other differences in the atmospheric settings, in particular the choice of cloud scheme. ACCESS1.3 is generally warmer in Eurasia in winter than ACCESS1.0, in some places changing the sign of the bias from the ERA-Interim reanalyses. This leads to earlier snowmelt, manifest as runoff, in Siberia in ACCESS1.3 than

Fig. 14. Diurnal amplitude of Australian mean seasonal screen temperature (°C) for ACCESS AMIP simulations; December/January/February (left column), June/July/August (right column), ACCESS1.0 (a, b), ACCESS1.3 (c, d), ERA-Interim analysis (e, f) and Bureau of Meteorology data (g, h).

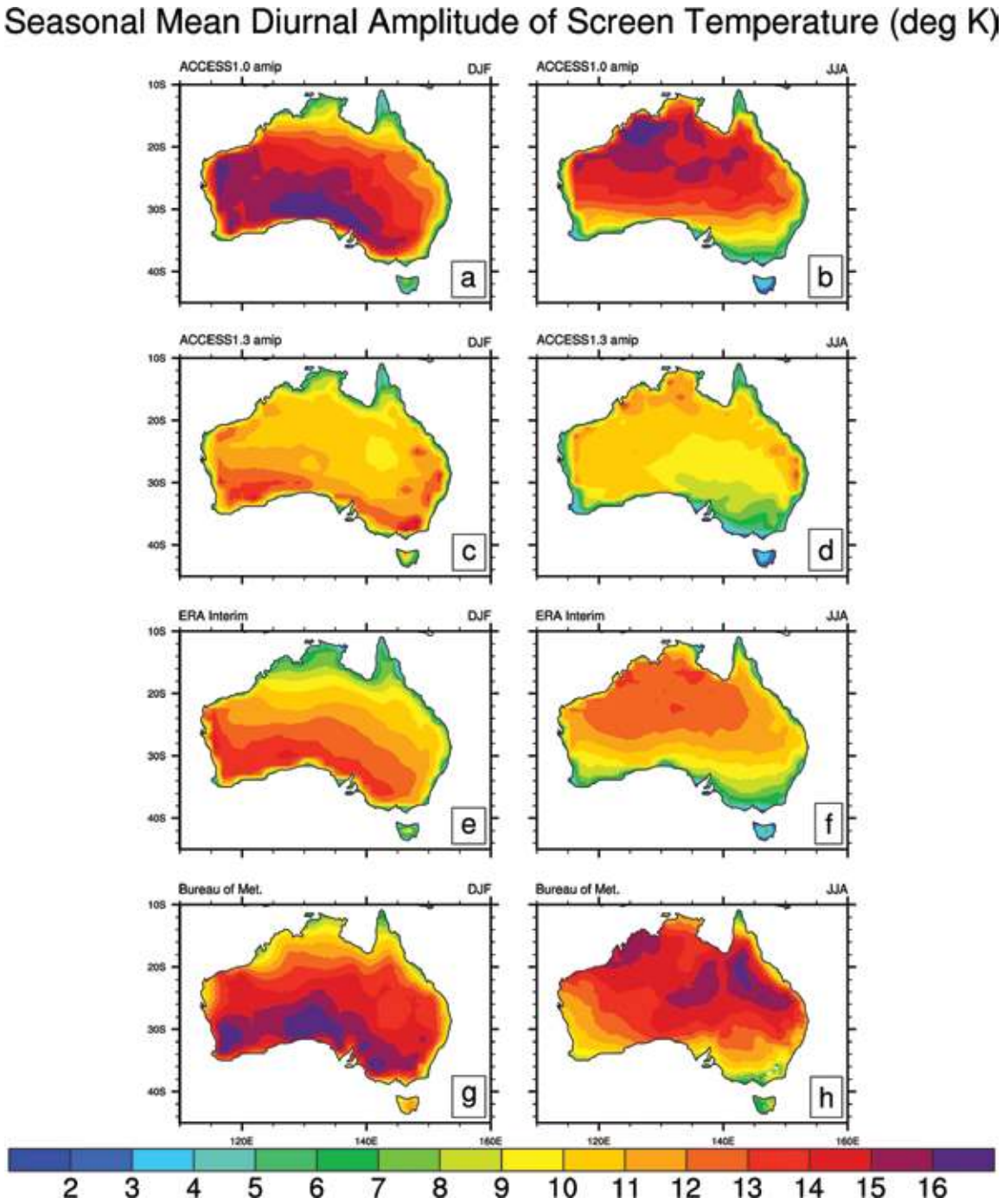

ACCESS1.0. One contributor to this difference may be lower simulated surface albedo in ACCESS1.3, than in ACCESS1.0. These lower albedos are due to an inconsistency between the prescribed soil albedo field and the radiation reflectance and transmission parameters in CABLE. However it appears that the albedo differences only play a secondary role; in summer ACCESS1.3 is cooler than ACCESS1.0 in east Siberia contrary to the lower albedos of ACCESS1.3.

The coupled model simulations moderate or amplify the biases seen in the atmosphere only cases, depending on nearby sea surface temperature biases. For example warm sea surface temperature biases in the southern ocean in the coupled model amplify the warm bias over Antarctica in DJF using ACCESS1.0. By contrast warm biases over northern land in summer are moderated by negative sea surface temperature biases in the northern mid-latitudes of

the Pacific and Atlantic.

Australian precipitation patterns are reproduced by both simulations but the precipitation over southwestern Australia is too low and in southeastern Australia the rainfall associated with flow over topography is absent. The 1.3A results for the diurnal amplitude range are more consistent with the diurnal amplitude from ERA-Interim while the 1.0A results are more consistent with the Bureau of Meteorology temperature dataset.

The number of differences between the atmospheric settings of ACCESS1.0 and ACCESS1.3 has made it difficult to attribute differences in the simulated climatology to the land surface scheme. Future work will document a series of test simulations in which CABLE and MOSES have been run with the same atmospheric settings and using the same land surface configuration (vegetation types and soil discretisation) as MOSES so that land surface processes can be compared cleanly. Further CMIP5 simulations will also be undertaken with the aim of upgrading CABLE to v2.0, improving the albedo simulation and testing the impact of changing the vegetation distribution in time. The biogeochemical submodel (CASA-CNP) will also be included allowing the land carbon cycle to be simulated.

Acknowledgments

This work has been undertaken as part of the Australian Climate Change Science Program, funded jointly by the Department of Climate Change and Energy Efficiency, the Bureau of Meteorology and CSIRO. The work was supported by the NCI National Facility at the ANU.

References

Abramowitz, G., Leuning, R., Clark, M. and Pitman, A. 2008. Evaluating the Performance of Land Surface Models. *J. Clim., 21,* 5468–81.

Abramowitz, G. 2012. Towards a public, standardized, diagnostic benchmarking system for land surface models. *Geosci. Model Dev., 5,* 819–27, doi:10.5194/gmd-5-819-2012.

Baumgartner , A. and Reichel, E. 1975. The world water balance, trans. By R. Lee, Elseviere Sience. Best, M. J., Pryor, M., Clark, D.B., Rooney, G.G., Essery, R.L.H., Ménard, C.B., Edwards, J.M., Hendry, M.A., Porson, A., Gedney, N., Mercado, L.M., Sitch, S., Blyth, E., Boucher, O., Cox, P.M., Grimmond, C.S.B. and Harding, R.J. 2011. The Joint UK Land Environment Simulator (JULES), model description—Part 1: Energy and water fluxes. *Geosci. Model Dev, 4,* 677–99, doi:10.5194/gmd-4-677-2011. URL http://www.geosci-model-dev.net/4/677/2011/.

Bi, D., Dix, M., Marsland, S., O'Farrell, S., Rashid, H.A., Uotila, P., Hirst, A.C., Kowalczyk, E.A., Golebiewski, M., Sullivan, A., Yan, H., Hanna, N., Franklin, C., Sun, Z., Vohralik, P., Watterson, I., Zhou, X., Fiedler, R., Collier, M., Ma, Y., Noonan, J., Stevens, L., Uhe, P., Zhu, H., Hill, R., Harris, C., Griffies, S. and Puri, K. 2013. The ACCESS Coupled Model: Description, Control Climate and Preliminary Validation. *Aus. Meteorol. Oceanogr. J.*, 63, 41–64.

Bierkens, M.F.P., Dolman, A.J., Troch P.A. 2008. Editors: Climate and the Hydrological Cycle, IAHS Special Publication 8.

Budyko, M.I.1978. *The heat balance of the Earth*, in: Gribbin, J. (ed), Climate Change, pp. 85–113, Cambridge University Press.

Bureau of Meteorology. 2000. Climatic Atlas of Australia – Rainfall

Clapp, R. and Hornberger, G. 1978. Empirical equations for some soil hydraulic properties. *Water Resources Research, 14,* 601–4.

Cosby, B., Hornberger, G., Clapp, R. and Ginn, T. 1984. A statistical exploration of the relationships of soil moisture characteristics to the physical properties of soils. *Water Resources Research, 20,* 682–90.

Cox, P., Betts, R., Bunton, C., Essery, P., Rowntree, R. and Smith, J. 1999. The impact of new land surface physics on the GCM simulation of climate and climate sensitivity. *Clim. Dyn., 15,* 183–203.

Cox, P. M. 2001. Description of the TRIFFID dynamic global vegetation model. Hadley Centre Technical Note 24, Met Office, UK, 2001.

Davies, T., Cullen, M.J.P., Malcolm, A.J., Mawson, M.H., Staniforth, A., White, A. A., and Wood, N. 2005. A new dynamical core for the Met Office's global and regional modelling of the atmosphere, *Q. J. R. Meteorol. Soc., 131,* 1759–82.

Dee, D.P., Uppala, S.M., Simmons, A.J., Berrisford, P., Poli, P. and others. 2011. The ERA-Interim reanalysis: configuration and performance of data assimilation system. *Q. J. R. Meteorol. Soc., 137,* 553–97.

Dix, M., Vohralik, P., Bi, D., Rashid, H.A., Marsland, S., O'Farrell, S., Uotila, P., Hirst, A.C., Kowalczyk, E.A., Sullivan, A., Yan, H., Franklin, C., Sun, Z., Watterson, Collier, M., Noonan, J., Stevens, L., Uhe, P. and Puri, K. 2013. The ACCESS Coupled Model: Documentation of core CMIP5 simulations and initial results. *Aust. Meteorol. Oceanogr. J.*, 63, 83–99.

Essery, R., Best, M. and Cox, P. 2001. MOSES 2.2 technical documentation. Hadley Centre technical note 30, Met. Office, Exeter, UK.

Franklin, C.N., Jakob, C., Dix, M., Protat A. and Roff, G. 2012. Assessing the performance of a prognostic and a diagnostic cloud scheme using single column model simulations of TWP-ICE. *Q. J. R. Meteorol. Soc, 138,* 734–54, doi: 10.1002/qj.954

Franklin, C.N., Sun, Z., Bi, D., Dix, M., Yan H. and Bodas-Salcedo, A. 2013. Evaluation of clouds in ACCESS using the satellite simulator Package COSP. Part I: Global, seasonal and regional cloud properties. *J. Geophys. Res., 118,* 732–48, doi: 10.1029/2012JD018469.

Global Soil Data Task Group. 2000. Global Gridded Surfaces of Selected Soil Characteristics (IGBP-DIS). [Global Gridded Surfaces of Selected Soil Characteristics (International Geosphere-Biosphere Programme – Data and Information System)]. Data set. Available on-line [http://www.daac.ornl.gov] from Oak Ridge National Laboratory Distributed Active Archive Center, Oak Ridge, Tennessee, U.S.A. doi:10.3334/ORNLDAAC/569, http://daac.ornl.gov/SOILS/guides/igbp-surfaces.html

Griffies, S.M., Harrison, M.J., Pacanowski, R.C. and Rosati, A. 2007. Ocean modelling with MOM. *Clivar Exchanges, 12,* 3–5, 13.

Henning, D. 1989. *Atlas of the Surface Heat Balance of the Continents*. Gerbruder Borntraeger, 402 pp.

Hewitt, H. T., Copsey, D., Culverwell, I.D., Harris, C.M., Hill, R.S.R., Keen, A.B., McLaren, A.J. and Hunke, E.C. 2011. Design and implementation of the infrastructure of HadGEM3: the next-generation Met Office climate modelling system. *Geosci. Model Dev., 4,* 223–53.

Hunke, E. C. and Lipscomb, W.H. 2008. *CICE: The Los Alamos Sea Ice Model. Documentation and Software User's Manual.* Version 4.0. T-3 Fluid Dynamics Group, Los Alamos National Laboratory, Tech. Rep. LA-CC-06-012.

Hurtt, G. C. et a. 2011. Harmonization of land-use scenarios for the period 1500–2100: 600 years of global gridded annual land-use transitions, wood harvest, and resulting secondary lands. *Climatic Change, 109,* 117–161, doi:10.1007/s10584-011-015

Jones, C.P. 2008. Ancillary file data sources, *Unified Model Documentation, Paper no 70, Version 10,* Met. Office, Exeter, UK.

Houldcroft, C.J., Grey,W.M.F., Barnsley, M., Taylor, C.M. and Los, S.O. 2009. New vegetation albedo parameters and global fields of background albedo derived from MODIS for use in climate model, *J. Hydrometeor. 10,* 193–8.

Kowalczyk, E.A., Wang, Y.P., Law, R.M., Davies, H.L., McGregor, J.L, and Abramowitz, G.S. 2006. The CSIRO Atmosphere Biosphere Land Exchange (CABLE) model for use in climate models and as an offline model. (CSIRO Marine and Atmospheric Research Paper; 013) Aspendale, Vic.: CSIRO Marine and Atmospheric Research. 43p.

Kumar, S.V., Peters-Lidard, C.D., Santanello, J., Harrison, K., Liu, Y., and Shaw, M. 2012. Land surface Verification Toolkit (LVT) – a generalized framework for land surface model evaluation, *Geosci. Model Dev., 5,* 869–86, doi:10.5194/gmd-5-869-2012.

Law, R.M., Kowalczyk, E.A. and Wang, Y.P. 2006. Using atmospheric CO_2 data to assess a simplified carbon-climate simulation for the 20th cen-

tury. *Tellus, 58B*, 427–37.

Lawrence, P.J., Feddema, J.J., Bonan, G.B., Meehl, G.A., O'Neill, B.C., Oleson, K.W., Levis, S., Lawrence, D.M., Kluzek, E., Lindsay K. and Thornton, P.E. 2012. Simulating the Biogeochemical and Biogeophysical Impacts of Transient Land Cover Change and Wood Harvest in the Community Climate System Model (CCSM4) from 1850 to 2100, *J. Clim., 25,* 3071–95, DOI: 10.1175/JCLI-D-11-00256.1.

Legates, D.R. and Willmott. C.J. 1990. Mean seasonal and Spatial Variability in gauge-corrected, global precipitation. *Int. J.Climatol., 10,* 111–27.

Leuning, R. 1995. A critical appraisal of a combined stomatal photosynthesis model for C3 plants. *Plant Cell Environ., 18,* 339–55, doi:10.1111/j.1365-3040.1995.tb00370.x.

Loveland, T.R., Reed, B.C., Brown, J.F., Ohlen, D.O., Z. Zhu, Z., Yang, L. and Merchant, J.W. 2000. Development of a global land cover characteristics database and IGBP DISCover from 1km AVHRR data. *Int. J. Remote Sensing, 21,* 1303–3330.

Luo, Y.Q., Randerson, J., Abramowitz, G., Bacour, C., Blyth, E., Carvalhais, N., Ciais, P., Dalmonech, D., Fisher, J., Friedlingstein, P, Hibbard, K., Hoffman, F., Huntzinger, D., Jones, C.D., Koven, K., Lawrence, D., Li, D.J., Mahecha, M., Niu, S.L., Norby, R., Piao, S.L., Qi, X., Peylin, P., Prentice, I.C.,. Riley, I., Reichstein, M., Schwalm, C., Wang, Y.P., Xia, Y., Zaehle, S. and Zhou, X.H. 2012. A framework of benchmarking land models. *Biogeosciences Discuss., 9,* 1899–944.

Marsland, S.J., Bi, D., Uotila, P., Fiedler, R., Griffies, S.M., Lorbacher, K., O'Farrell, S., Sullivan, A., Uhe, P., Zhou, X., Hirst, A.C. 2013. Evaluation of ACCESS Climate Model ocean diagnostics in CMIP5 simulations, *Aust. Met. Oceanogr. J.,* 63, 101–19.

Martin, G.M., Bellouin, N., Collins, W.J., Culverwell, I.D., Halloran, P.R., Hardiman, S.C., Hinton, T.J., Jones, C.D., McDonald, R.E., McLaren, A.J., O'Connor, F.M., Roberts, M.J., Rodriguez, J.M., Woodward, S., Best, M.J., Brooks, M.E., Brown, A.R., Butchart, N., Dearden, C., Derbyshire, S.H., Dharssi, I., Doutriaux-Boucher, M., Edwards, J.M., Falloon, P.D., Gedney, N., Gray, L.J., Hewitt, H.T., Hobson, M., Huddleston, M.R., Hughes, J., Ineson, S., Ingram, W.J., James, P.M., Johns, T.C., Johnson, C.E., Jones, A., Jones, C.P., Joshi, M.M., Keen, A.B., Liddicoat, S., Lock, A.P., Maidens, A.V., Manners, J.C., Milton, S.F., Rae, J.G.L., Ridley, J.K., Sellar, A., Senior, C.A,., Totterdell, I.J., Verhoef, A., Vidale, P.L. and Wiltshire, A. 2011. The HadGEM2 family of Met Office Unified Model climate configurations. *Geosci. Model Dev., 4,* 723–57.

Moody, E.G., King, M.D., Platnick, S., Schaaf, C.B. and Gao, F. 2005. Spatially complete global spectral surface albedos: value-added datasets derived from Terra MODIS land products. *IEEE Transactions on Geoscience and Remote Sensing, 43,* 144–58.

Oak Ridge National Laboratory Distributed Active Archive Center (ORNL DAAC). 2011. FLUXNET Web Page. Available online [http://fluxnet.ornl.gov] from ORNL DAAC, Oak Ridge, Tennessee, U.S.A. Accessed November 5, 2011.

Pitman, A.J. 2003. The evolution of, and revolution in, land surface schemes designed for climate models, *Int. J. Climatol., 23,* 479–510, doi:10.1002/joc.893.

Oki, T. and Sud, Y.C. 1998. Design of total runoff integrating pathways (trip) a global river channel network. *Earth Interact., 2,* 1–37. doi: http://dx.doi.org/10.1175/1087-3562(1998)002<0001:DOTRIP>2.3.CO;2

Puri, K., Dietachmayer, G., Steinle, P., Dix, M., Rikus, L., Logan, L., Naughton, M., Tingwell, C., Xiao, Y., Barras, V., Bermous, I., Bowen, R., Deschamps, L., Franklin, C., Fraser, J., Glowacki, T., Harris, B., Lee, J., Le, T., Roff, G., Sulaiman, A., Sims, H., Sun, X., Sun, Z., Zhu, H., Chattopadhyay, M. and Engel, C. 2013. Implementation of the initial ACCESS Numerical Weather Prediction system, *Aust. Meteorol. Oceanogr. J.,* in press.

Raupach, M.R., Finkele, K. and Zhang, L. 1997. SCAM (Soil-Canopy-Atmosphere Model): description and comparisons with field data. *CSIRO Centre for Environmental Mechanics Tech. Rep. 132.*

Rashid, H.A., Sullivan, A., Hirst, A.C., Bi, D. , Zhou, X. and Marsland, S.J. 2013. Evaluation El Nino-Southern Oscillation in ACCESS coupled model simulations for CMIP5. *Aust. Meteorol. Oceanogr. J.,* 63, 161–80.

Risbey, J.S., McIntosh, P.C., Pook, M.J., Rashid, H.A. and Hirst. A.C. 2011. Evaluation of rainfall drivers and teleconnctions in an ACCESS AMIP run. *Aust. Meteorol. Sand Ocean. J., 61,* 91–105.

Shukla, J. and Mintz, Y. 1982. Influence of land surface evapotranspiration on the Earth's climate. *Science, 215,*1498–501, doi:10.1126/science.215.4539.1498.

Valcke, S. 2006. OASIS3 User Guide (prism_2-5). CERFACS Technical Report TR/CMGC/06/73, PRISM Report No 3, Toulouse, France.

Smith, R.N.B. 1990. A scheme for predicting layer clouds and their water contents in a general circulation model. *Q. J. R. Meteorol. Soc., 116,* 435–60.

Smith, T.M., Reynolds, R., Peterson, T. C. and Lawrimore, J. 2008. Improvements to NOAA's historical merged land-surface temperature analysis (1880–2006), *J. Climate, 21,* 2283–96, doi:10.1175/2007JCLI2100.1.

Tan, A., Adam, J.C. and Lettenmair, P. 2011. Change in spring snowmelt timing in Eurasian Arctic rivers, *J. Geophys. Res.-Biogeo., 116,* doi:10.1029/2010JD014337.

Wang, Y.P. and Leuning, R. 1998. A two-leaf model for canopy conductance, photosynthesis and partitioning of available energy I. Model description and comparison with a multi-layered model. *Agric. Forest Meteorol., 91,* 89–111.

Wang, Y.P., Law, R.M., and Pak, B. 2010. A global model of carbon, nitrogen and phosphorus cycles for the terrestrial biosphere. *Biogeosciences, 7,* 2261–82, doi:10.5194/bg-7-2261-2010.

Wang, Y.P., Kowalczyk, E.A., Leuning, R., Abramowitz, G., Raupach, M.R., Pak, B., van Gorsel, E. and Luhar, A. 2011. Diagnosing errors in a land surface model (CABLE) in the time and frequency domains. *J. Geophys. Res.-Biogeo., 116.*

Wilson, M.F. and Henderson-Sellers, A. 1985. A global archive of land cover and soils data for use in general circulation climate models. *J. Climatol., 5,* 119–43.

Wilson, D.R., Bushell, A.C., Kerr-Munslow, A.M., Price J.D.and Morcrette., C.J. 2008. PC2: A prognostic cloud fraction and condensation scheme. I: Scheme description. *Q. J. R. Meteorol. Soc., 134,* 2093–107.

Yang, W., Shabanov, N.V., Huang, D., Wang, W., Dickinson, R.E. Nemani, R.R., Knyazikhin, Y., Myneni, R.B. 2006. Analysis of leaf area index products from combination of MODIS Terra and Aqua data. *Remote Sensing of Environment, 104,* 297–312.